

See discussions, stats, and author profiles for this publication at: <https://www.researchgate.net/publication/227993321>

Templated Self-Assembly of Colloidal Nanoparticles Controlled by Electrostatic Nanopatterning on a Si₃N₄/SiO₂/Si Electret

ARTICLE *in* ADVANCED MATERIALS · MAY 2006

Impact Factor: 17.49 · DOI: 10.1002/adma.200501542

CITATIONS

49

READS

9

5 AUTHORS, INCLUDING:



Shien-Der Tzeng

National Dong Hwa University

24 PUBLICATIONS 402 CITATIONS

SEE PROFILE



S. Gwo

National Tsing Hua University

91 PUBLICATIONS 1,898 CITATIONS

SEE PROFILE

DOI: 10.1002/adma.200501542

Templated Self-Assembly of Colloidal Nanoparticles Controlled by Electrostatic Nanopatterning on a $\text{Si}_3\text{N}_4/\text{SiO}_2/\text{Si}$ Electret**

By Shien-Der Tzeng, Kuan-Jiuh Lin, Jung-Chih Hu, Lih-Juann Chen, and Shangjr Gwo*

Metal and semiconductor nanoparticles display fascinating size-dependent structural, electronic, optical, magnetic, and chemical properties, which make them promising materials to be tailored and functionalized as fundamental building blocks for emerging nanotechnology applications.^[1,2] Because of the strong dependence of nanoparticle properties on their quantum-scale dimensions, the synthesis of nanoparticles with a small size and shape variation is of key importance. At present, size-, shape-, composition-, and surface-chemistry-controlled nanoparticles can be synthesized by colloidal-solution methods for a wide range of materials.^[3,4] Furthermore, strategies have been developed in which monodispersed nanoparticles can form self-assembled, long-range nanoparticle lattices (2D and 3D) under appropriate conditions.^[1,2,5,6] The next important challenge for emerging nanotechnological applications (chemical and biological sensing, electronics, optoelectronics) is to perform controlled and hierarchical self-assembly of monodispersed nanoparticles from the solution phase into ordered and specifically designed nanoparticle structures immobilized on solid-surface templates. In this paper, we report an approach for controlled assembly of metal (Au) and semiconducting (CdSe/ZnS core/shell) thiol-terminated nanoparticles onto electrically patterned $\text{Si}_3\text{N}_4/\text{SiO}_2/\text{Si}$ (NOS) electret films with an unprecedented resolution.

In the past few years, several important breakthroughs in scanning-probe-based lithographic techniques using tip-induced local electrochemical reactions of self-assembled monolayers (SAMs)^[7–10] or tip-induced local-transport processes, such as dip-pen nanolithography,^[11,12] were developed

for fabricating surface templates, which can be used to assemble nanoparticles on solid supports. In these techniques, the patterning process is realized by molecular reaction or transport through a water meniscus that naturally occurs between the tip and sample under ambient conditions. Therefore, the typical resolution and writing speed of such techniques is controlled by parameters such as probe scan speed, temperature, humidity, and molecule type. Furthermore, the reaction or transport rate is limited by the reaction or ink-transport process. As a result, these types of lithographic mechanism limit the line-writing speed to the range $0.1\text{--}10\text{ }\mu\text{m s}^{-1}$ and the dot-writing time to the range of a few milliseconds to tens of seconds per dot (size-dependent) under ambient conditions.^[7–12] Recently, electrostatic-force-based assembly of nanoparticles has been proposed as a general, precise, and reliable methodology for such purposes.^[13–22] In the most direct type of electrostatic-force-based assembly, charge patterns are created by scanning-probe or microcontact charging techniques onto electret materials via electron- or hole-tunneling processes.^[16–20] As the electret materials can retain electric charge or polarization for a long time, these charge patterns can be used as templates for assembling charged or polarizable nanoparticles. The major advantage of electrostatic lithography is that, in contrast to diffusion processes, the patterning speed can be enhanced over three orders of magnitude. However, because electrostatic forces scale with surface area and particle size, nanoscale electrostatic assembly of nanoparticles is a formidable task.

Xerography (a form of electrophotography) is currently one of the prevailing methods for pattern generation or replication, with $\sim 100\text{ }\mu\text{m}$ resolution. In this process, charged toner particles (with diameters in the range of several micrometers) are attracted by electrostatic-charge patterns (latent electrostatic images) created on a photosensitive electret, and the images are developed with these toner particles.^[23,24] Very recently, nanoscale xerography (nanoxerography) using an electrical microcontact printing process^[16,18–20] or a scanning-probe-based process^[14,17] was proposed as a means for nanoscale pattern generation or replication.

In this work, by using an optimized electret structure (NOS dielectric stack),^[25–28] improved local-charging conditions under high vacuum, and chemically modified nanoparticles (5 nm thiol-terminated gold colloids, see the literature^[29] and the Experimental section for the synthesis procedure), we are able to perform selective attachment of gold colloidal nanoparticles onto the patterned electret in a toluene solution at a resolution of $\sim 30\text{ nm}$. Furthermore, in our process, only a

[*] Prof. S. Gwo, Dr. S.-D. Tzeng
Department of Physics and Materials Science Center
National Tsing-Hua University
Hsinchu 300, Taiwan (ROC)
E-mail: gwo@phys.nthu.edu.tw

Prof. K.-J. Lin
Department of Chemistry and Center of Nanoscience and
Nanotechnology
National Chung-Hsing University
Taichung 402, Taiwan (ROC)

Dr. J.-C. Hu, Prof. L.-J. Chen
Department of Materials Science and Engineering
National Tsing-Hua University
Hsinchu 300, Taiwan (ROC)

[**] This work was supported by the National Nanoscience and Nanotechnology Project (NSC 94-2120-M-007-002). We thank J.-L. Hsieh of Nano Device Laboratory (NDL) for the supply of NOS samples. Supporting Information is available online from Wiley InterScience or from the author.

monolayer of nanoparticles is assembled in one step, allowing better structural control and the possibility of forming hierarchical nanoparticle structures.

Electrostatic nanopatterning was achieved by electrostatic force microscopy (EFM)^[28,30] under high-vacuum conditions ($\sim 1 \times 10^{-6}$ Torr, 1 Torr = 133 Pa), which allows higher charge detection sensitivity and patterning resolution than that operated under ambient conditions.^[28] It also prevents the local-charging process from the effects of probe-induced anodic oxidation.^[31] Ultrathin NOS electrets were prepared by thermal oxidation and low-pressure chemical vapor deposition on p-type Si(001) wafers with layer thicknesses (nitride/oxide) of 30 and 22 Å, respectively. An ultrathin dielectric structure effectively confines the electric field between the EFM tip and the conductive substrate, so that an ultrahigh areal density of charge bits can be achieved. Besides, the writing speed can be very high with a low writing voltage (5–10 V). In this way, we succeeded in demonstrating an ultrahigh areal density (up to 500 Gbit in.⁻², one order of magnitude higher than the previously reported charge-writing densities) and fast writing speed. In addition to these advantages, direct quantitative determination of retention times, trapping energies, and injection-tunneling barriers for electrons and holes can be obtained using the technique of variable-temperature EFM.^[32] A high charge-retention time (longer than ten years at room temperature) can be extrapolated from the variable-temperature EFM study.

Figure 1a shows the schematic of the charge sensing and manipulation setup. The trapped charges were measured by EFM in intermittent-contact mode, with both mechanical and electrical modulations. By using a dual-modulation scheme at

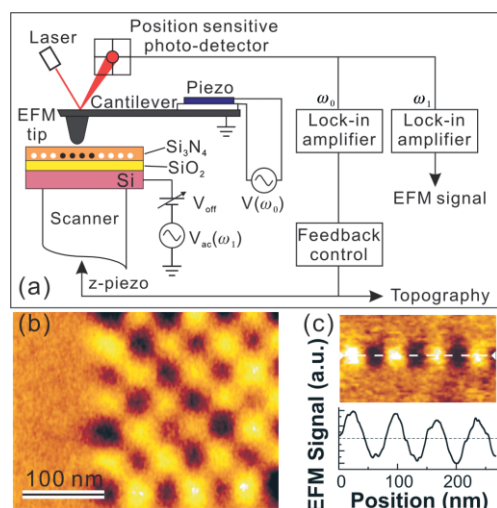


Figure 1. Charge sensing and manipulation with nanoscale resolution. a) Schematic drawing of the charge sensing and manipulation setup. b) EFM images of high areal density (~ 500 Gbit in.⁻²) charge bits injected into an NOS (30 Å/22 Å) ultrathin film. The darker and brighter regions were injected with electrons and holes, respectively. c) EFM image and cross-sectional EFM line profile of charge bits. These results show that charge bits can be written in less than 10 μ s with a minimum feature size of ~ 30 nm.

two noninterfering modulation frequencies, the atomic force microscopy (AFM) surface topography and an EFM charge image can be simultaneously obtained. The vibrating frequency (ω_0) of the tip was about 60 kHz (slightly below the resonant frequency of the cantilever), and the typical vibration amplitude was about 100 nm. The DC offset voltage (V_{off}) and AC modulation voltage (V_{ac}) for EFM measurements on our NOS films were typically -700 and 500 mV, respectively. The electrical modulation frequency (ω_1) was 20–80 kHz (depending on the mechanical response of individual EFM probes). To manipulate (write, erase, and rewrite) charges, a DC sample bias was applied between the conductive silicon substrate and the EFM tip, allowing electrons or holes to tunnel from the tip into the charge-trapping sites of the NOS electret film. In principle, local charging could be done under both intermittent-contact and contact modes. For this work, during the process of electrostatic patterning, we switched the operation mode to the contact mode using the same EFM probe. Figures 1b and c are EFM images of charge bits injected into NOS samples. The darker and brighter regions result from trapped electrons and holes, respectively. Figure 1c shows the cross-sectional EFM line profile of the charge bits. These charge bits were written by a ± 10 V square-wave sample bias (repetition rate = 60 kHz), with a tip moving speed of ~ 4.3 mm s⁻¹. These results show that charge bits can be written in less than 10 μ s with a minimum feature size of ~ 30 nm. It should be noted that the achieved writing speed in this work is by no means a limit of this process. Significantly higher writing speeds could be realized with more optimized electronics and a tip/sample scanner specifically designed for electrostatic nanopatterning.

We found that charges can be easily written and erased on the NOS without affecting the sample topography. The EFM image shown in Figure 2a is a charge pattern created by alternate writing and erasing of charges, with the patterning sequence shown in the upper part. Judging from the simultaneously obtained AFM image, there is no topographic change on the same sample area. In addition, by using the technique of lateral force microscopy (LFM) for friction force imaging, we found no chemical contrast between locally charged and as-grown NOS surfaces (Supporting Information, Fig. S1). The absence of observable topography and friction-force contrasts after charge injection indicates that probe-induced local oxidation did not occur under our experimental conditions. By using this method (scanning charge lithography, SCL), we have been able to generate complex charge features with trapped electrons and holes, including lines, circles, and dots. In principle, SCL can be used to pattern almost any 2D features (some examples are shown in Fig. 2b). The densities of trapped charges can also be controlled to induce a surface-potential change in the range of -1.0 to $+1.0$ V compared to that of the uncharged surface. These properties are very helpful for controlling the selective adsorption of charged or polarizable nanoparticles.

To guide attachment of nanoparticles to specific sites on a locally charged surface with nanometer resolution, two kinds

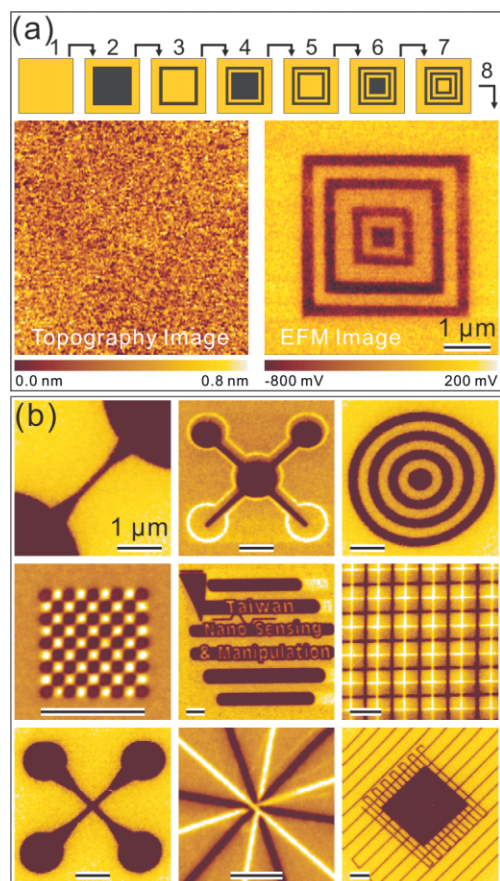


Figure 2. Erasable/rewritable charge patterns with excellent patterning flexibility. a) EFM image (lower right-hand side) showing a charge pattern created by alternate writing and erasing of charges. The patterning sequence is shown in the upper panel. The color scale in the EFM image represents the magnitude of surface potential. There is no topographic change on the same sample area (lower left-hand side). b) Both positive and negative charges can be written with various charge patterns. Scale bars represent 1 μm . The densities of trapped charges can be controlled to induce a surface-potential change in the range -1.0 to $+1.0$ V compared to that of the uncharged surface.

of attractive interactions are exploited as the driving forces for the formation of self-assembled nanoparticle structures. The first kind is electrostatic attraction between the charged surface regions and the charged/polarizable nanoparticles in solutions. The second kind is the like-charge attraction induced by geometrical confinement^[33] between nanoparticles on the charged surface regions, which would allow the formation of close-packed, ordered nanoparticle monolayer structures. Besides these attractive interactions, the thiol surface termination on nanoparticles also turns out to be critical to prevent agglomeration of nanoparticles onto the charged regions because of the hydrophobic nature of thiol encapsulation. It also prevents them from adsorbing onto the uncharged, as-grown NOS surface.

Figure 3a is a schematic presentation of three steps used to perform selective adsorption of dodecanethiol [$\text{CH}_3\text{-(CH}_2\text{)}_{11}\text{SH}$]-encapsulated gold colloidal nanoparticles in a tol-

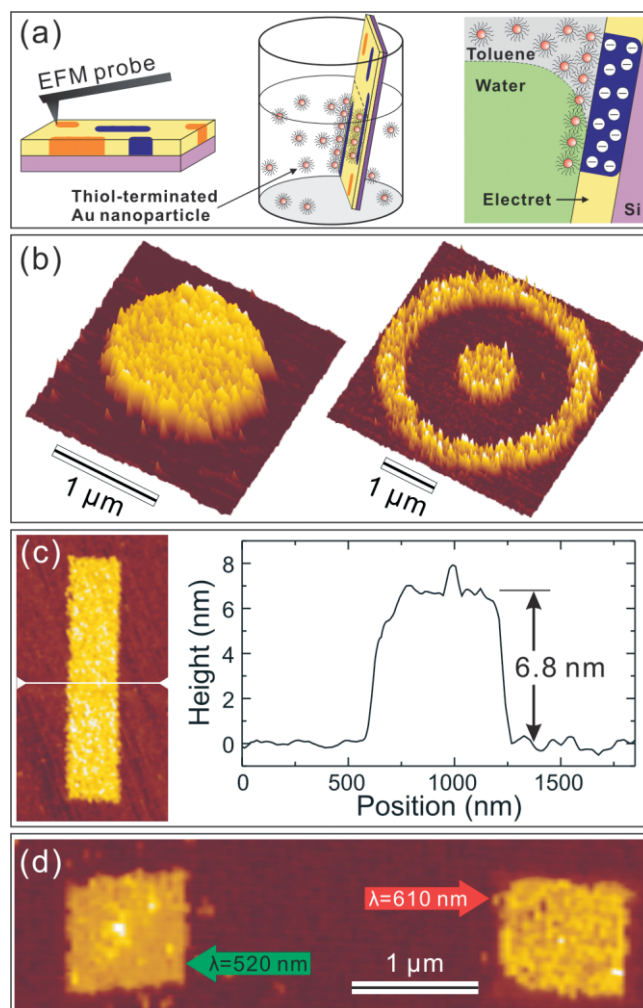


Figure 3. Selective adsorption of thiol-terminated gold and CdSe/ZnS nanoparticles. a) Schematic of three steps to perform selective adsorption of gold colloidal nanoparticles in a toluene solution, by using electrostatic patterns created on NOS. b) 3D AFM images of selectively adsorbed gold nanoparticles. c) Cross-sectional topographic height of selectively adsorbed gold nanoparticles, showing that only a monolayer of nanoparticles can be formed on the negatively charged surface regions. d) AFM image of selectively adsorbed CdSe/ZnS core/shell nanoparticles. Two kinds of thiol-terminated CdSe/ZnS nanoparticles, corresponding to photoluminescence wavelengths of ~ 610 nm (red) and ~ 520 nm (green), were successively adsorbed by repeating the selective-adsorption procedure at different sample areas.

uene solution. At first, charge patterns are created by EFM under high vacuum. In the second step, the local negatively charged sample is removed from the EFM vacuum chamber and immediately dipped into the toluene solution of thiol-terminated gold nanoparticles. The immersion time is typically 3–10 s. In the last step, the sample is removed from the nanoparticle solution and is immediately dipped into deionized water to rinse off the residual colloidal solution. The loosely adsorbed nanoparticles can be separated from the sample surface by this process.

In our experiments, the uncharged surface showed no sign of nanoparticle adsorption. In addition, we found that the

negatively charged surface regions attracted dodecanethiol-encapsulated gold nanoparticles, while the positively charged surface regions tended to repel gold nanoparticles. Therefore, the present mechanism of selective area adsorption of gold nanoparticles is similar to the previously reported electrophoretic deposition of gold-nanoparticle monolayers on carbon-coated surfaces (in that case, complete surface coverage without control of deposition sites^[5]). Figure 3b shows AFM images after selective-area adsorption of gold nanoparticles onto various negatively charged patterns. The deposition of positively charged nanoparticles from the toluene suspension occurs very specifically on the negatively charged regions of the sample surface, inferring that they are positively charged (Supporting Information, Fig. S2). We have also confirmed that positively charged patterns could not induce the selective adsorption of gold nanoparticles (Supporting Information, Fig. S3). The AFM image and cross-sectional topographic height of selectively adsorbed gold nanoparticles on a rectangular charge pattern are shown in Figure 3c. The latter indicates that only a monolayer (~ 6.8 nm) of adsorbed nanoparticles can be formed on the negatively charged surface regions.

This method can also be applied to semiconductive or dielectric nanoparticles. For example, Figure 3d shows the AFM image of selective area adsorption (two successive selective area adsorption steps in different colloidal solutions) of CdSe/ZnS core/shell nanoparticles with photoluminescence wavelengths of ~ 610 nm (red) and ~ 520 nm (green). The CdSe core sizes listed in the specifications of the commercial provider are ~ 4.5 nm (red) and ~ 2.1 nm (green). The topographic heights, as measured by AFM, are ~ 5 – 6 nm and ~ 4 – 5 nm, respectively. We found that the selectively adsorbed nanoparticle monolayers could be intentionally disintegrated by strong sonication in water (unlike the case of selectively adsorbed Au nanoparticles) or by mechanical scratching using an AFM tip. Compared to the dielectric solvent medium (toluene), CdSe/ZnS core/shell nanoparticles are more polarizable and conductive. Thus, they experience a dielectrophoretic force that produces net movement in the direction of increasing electric field. It was found that both positively and negatively charged regions could selectively adsorb CdSe/ZnS core/shell nanoparticles. However, the degree of selective adsorption onto a negatively charged surface is better (more densely packed), indicating that CdSe/ZnS core/shell nanoparticles in toluene are also slightly positively charged. In our experiments with Au and CdSe/ZnS core/shell nanoparticles, toluene is a particularly suitable solvent for both electrophoresis and dielectrophoresis because of its low dielectric constant ($\epsilon = 2.4$ at room temperature, for comparison, see Supporting Information, Fig. S4). In Figure 3d, the red-light-emitting nanoparticles were assembled first; the sample was then transferred to vacuum again to write a new charge pattern before selectively adsorbing the green-light-emitting nanoparticles. Thus, it clearly demonstrates that nanoparticles with diverse properties can be successively adsorbed onto a single template surface by repeating the selective-adsorption procedure with different solutions of nanoparticles.

Figure 4 displays scanning electron microscopy (SEM) images of selectively adsorbed gold-nanoparticle structures. The SEM images show that thiol-terminated gold nanoparticles

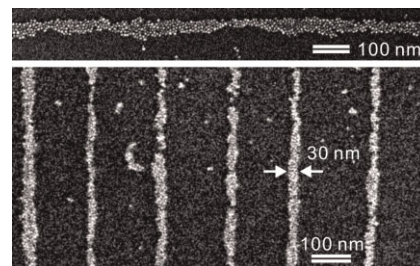


Figure 4. SEM images of selectively adsorbed gold nanoparticles. The images show that thiol-terminated 5 nm gold nanoparticles can be selectively adsorbed onto negatively charged line patterns at a line-width resolution of 30 nm. These gold nanoparticles are close-packed with a well-defined gap distance, which is determined by the length of the thiol molecules self-assembled on the gold-nanoparticle surface.

can be selectively adsorbed onto negatively charged line patterns at a line-width resolution of 30 nm. The SEM-measured interparticle distance is 7.81 ± 0.45 nm, only slightly larger than the nanoparticle height (~ 6.8 nm), as determined from Figure 3c. Considering the thickness of dodecanethiol capping (~ 1.3 nm)^[34] and the average diameter of the gold nanoparticle core (~ 5 nm), these gold nanoparticles form a close-packed monolayer with a well-defined gap distance between the nanoparticles, which is determined by the thickness of the thiol molecules on the Au-nanoparticle surface.

The present methodology for electrostatic-force-based assembly of colloidal nanoparticles can also be applied to parallel processes, either by applying flexible micropatterned electrodes as the charging stamps^[13,15,16,18–20] or by using various types of scanning-probe arrays.^[35–37] By comparison, the stamping method has the advantages of high process throughput and good size scalability. On the other hand, the methods based on scanning-probe arrays can create charge patterns arbitrarily during the lithographic step, which allows more process flexibility.

In summary, a methodology is described here for the controlled assembly of colloidal nanoparticles onto an electrically nanopatterned electret film. These absorbed nanoparticles can pack closely into monolayered structures at an unprecedented spatial resolution (~ 30 nm). Selective adsorption of both metal (gold) and semiconducting (CdSe/ZnS core/shell) thiol-terminated nanoparticles has been demonstrated. Furthermore, it is possible to selectively and successively adsorb nanoparticles with diverse properties onto a single template. These unique processing properties (dual polarity/reversible charging, hierarchical processing, and solution-phase compatibility) along with the lithographic advantages (high resolution and fast writing) allow the present methodology to become a promising approach for constructing specifically designed nanoparticle structures.

Experimental

Fabrication of NOS Electret: The silicon oxide and silicon nitride thin films in the NOS structure were formed by thermal oxidation (at 900 °C) and low-pressure chemical vapor deposition (at 750 °C) on 6 in. p-type Si(001) wafers, following the standard fabrication processes for Si microelectronics. The layer thicknesses of nitride and oxide thin films were measured by ellipsometry.

Electrostatic Force Microscopy: We used an environment-controlled AFM/EFM system (Seiko Instruments, SPA-300HV) with a conducting probe tip to inject charges into the NOS electret films by applying a voltage on the p-type silicon substrate. The probes used in this work were PtIr-coated Si tips with a typical tip radius ~ 20 nm. The force constant and resonant frequency of the probes were about 2.8 N m^{-1} and 60 kHz, respectively. The operating vacuum pressure was $\sim 1 \times 10^{-6}$ Torr, and the pumping time was typically less than one hour with a magnetically levitated turbo pump.

Preparation of Dodecanethiol-Terminated Gold Nanoparticles: The solution of thiol-terminated 5 nm diameter gold nanoparticles in toluene was prepared by using the two-phase method [29], which can be described briefly as the following. First, an aqueous solution of hydrogen tetrachloroaurate (HAuCl_4 , 30 mL, 30 mM) was mixed with a solution of tetraoctylammonium bromide $[(\text{C}_8\text{H}_{17})_4\text{NBr}]$ (TOAB), phase transfer agent, 80 mL, 50 mM] in toluene and stirred vigorously until all the AuCl_4^- ions were transferred into the organic phase. After adding dodecanethiol ($\text{C}_{12}\text{H}_{25}\text{SH}$, stabilizing agent, 170 mg) to the organic phase, an aqueous solution of sodium borohydride (NaBH_4 , reducing agent, 25 mL, 400 mM) was slowly added and vigorously stirred for 3 h. Finally, the organic phase was separated and size-selective precipitation in a centrifuge was applied to narrow the size distribution of the thiol-terminated gold nanoparticles. An alternative preparation method utilized commercially available gold nanoparticles (~ 5 nm in size, water soluble, citrate-stabilized) from Sigma-Aldrich (G1402). A toluene solution of dodecanethiol (10 mL, 50 mM) was mixed with the aqueous gold colloidal solution (5 mL, without any dilution). A TOAB aqueous solution (5 mL, 50 mM) was then added to the mixed solution. Under stirring, the gold nanoparticles were transferred into the organic phase and terminated by dodecanethiol molecules [38]. The resulting positive charge on the gold particles might be related to the positively charged TOA^+ surfactant used to transfer the particles from water to toluene. The concentration of gold colloids used for our adsorption experiments was about $5 \mu\text{g mL}^{-1}$.

Preparation of Thiol-Terminated CdSe/ZnS Core/Shell Nanoparticles: Two solutions of thiol-terminated core/shell CdSe/ZnS nanoparticles with photoluminescence wavelengths of ~ 610 nm (red) and ~ 520 nm (green) in toluene were prepared. The commercially available toluene solutions of CdSe/ZnS nanoparticles without thiol termination were purchased from Evident Technologies. To prepare thiol-terminated CdSe/ZnS nanoparticles ($\lambda \approx 610$ nm), a diluted toluene solution of nanoparticles (4 mL, concentration $\approx 24 \mu\text{g mL}^{-1}$) was mixed with a toluene solution of octanethiol $[\text{CH}_3(\text{CH}_2)_7\text{SH}]$, 4 mL, 32 mM]. To prepare thiol-terminated CdSe/ZnS nanoparticles ($\lambda \approx 520$ nm), a diluted toluene solution of nanoparticles (4 mL, concentration $\approx 14 \mu\text{g mL}^{-1}$) was mixed with a toluene solution of dodecanethiol $[\text{CH}_3(\text{CH}_2)_{11}\text{SH}]$, 4 mL, 10 mM]. These mixed solutions were kept at room temperature for more than 24 h before the selective-area-adsorption experiments.

Received: July 26, 2005
Final version: January 10, 2006

- [1] C. B. Murray, C. R. Kagan, M. G. Bawendi, *Annu. Rev. Mater. Sci.* **2000**, 30, 545.
- [2] A. N. Shipway, E. Katz, I. Willner, *ChemPhysChem* **2000**, 1, 18.
- [3] V. F. Puentes, K. M. Krishnan, A. P. Alivisatos, *Science* **2001**, 291, 2115.
- [4] Y. Sun, Y. Xia, *Science* **2002**, 298, 2176.
- [5] M. Giersig, P. Mulvaney, *Langmuir* **1993**, 9, 3408.
- [6] R. P. Andres, J. D. Bielefeld, J. I. Henderson, D. B. Janes, V. R. Kolagunta, C. P. Kubiak, W. J. Mahoney, R. G. Osifchin, *Science* **1996**, 273, 1690.
- [7] H. Sugimura, N. Nakagiri, *Langmuir* **1995**, 11, 3623.
- [8] H. Sugimura, N. Nakagiri, *J. Am. Chem. Soc.* **1997**, 119, 9226.
- [9] R. Maoz, E. Frydman, S. R. Cohen, J. Sagiv, *Adv. Mater.* **2000**, 12, 725.
- [10] S. Liu, R. Maoz, J. Sagiv, *Nano Lett.* **2004**, 4, 845.
- [11] R. D. Piner, J. Zhu, F. Xu, S. H. Hong, C. A. Mirkin, *Science* **1999**, 283, 661.
- [12] D. S. Ginger, H. Zhang, C. A. Mirkin, *Angew. Chem. Int. Ed.* **2004**, 43, 30.
- [13] J. Tien, A. Terfort, G. M. Whitesides, *Langmuir* **1997**, 13, 5349.
- [14] W. M. D. Wright, D. G. Chetwynd, *Nanotechnology* **1998**, 9, 133.
- [15] J. Aizenberg, P. V. Braun, P. Wiltzius, *Phys. Rev. Lett.* **2000**, 84, 2997.
- [16] H. O. Jacobs, G. M. Whitesides, *Science* **2001**, 291, 1763.
- [17] P. Mesquida, A. Stemmer, *Adv. Mater.* **2001**, 13, 1395.
- [18] H. O. Jacobs, S. A. Campbell, M. G. Steward, *Adv. Mater.* **2002**, 14, 1553.
- [19] C. R. Barry, N. Z. Lwin, W. Zheng, H. O. Jacobs, *Appl. Phys. Lett.* **2003**, 83, 5527.
- [20] C. R. Barry, J. Gu, H. O. Jacobs, *Nano Lett.* **2005**, 5, 2078.
- [21] H. Fudouzi, M. Kobayashi, N. Shinya, *J. Nanopart. Res.* **2001**, 3, 193.
- [22] H. Fudouzi, M. Kobayashi, N. Shinya, *Adv. Mater.* **2002**, 14, 1649.
- [23] D. M. Pai, B. E. Springett, *Rev. Mod. Phys.* **1993**, 65, 163.
- [24] G. M. Sessler, J. E. West, in *Electrets*, Vol. 1 (Ed: G. M. Sessler), 3rd ed., Laplacian Press, Morgan Hill, CA **1998**, Ch. 7.
- [25] R. C. Barrett, C. F. Quate, *J. Appl. Phys.* **1991**, 70, 2725.
- [26] H. J. Mamin, B. D. Terris, L. S. Fan, S. Hoen, R. C. Barrett, D. Rugar, *IBM J. Res. Dev.* **1995**, 39, 681.
- [27] I. Fujiwara, S. Kojima, J. Seto, *Jpn. J. Appl. Phys. Part 1* **1996**, 35, 2764.
- [28] S.-D. Tzeng, C.-L. Wu, Y.-C. You, T. T. Chen, S. Gwo, H. Tokumoto, *Appl. Phys. Lett.* **2002**, 81, 5042.
- [29] M. Brust, M. Walker, D. Bethell, D. J. Schiffrin, R. Whyman, *J. Chem. Soc. Chem. Commun.* **1994**, 801.
- [30] H. O. Jacobs, A. Stemmer, *Surf. Interface Anal.* **1999**, 27, 361.
- [31] F. S.-S. Chien, J.-W. Chang, S.-W. Lin, Y.-C. Chou, T. T. Chen, S. Gwo, T.-S. Chao, W.-F. Hsieh, *Appl. Phys. Lett.* **2000**, 76, 360.
- [32] S.-D. Tzeng, S. Gwo, unpublished.
- [33] Y. Han, D. G. Grier, *Phys. Rev. Lett.* **2003**, 91, 038302.
- [34] H. A. Biebuyck, C. D. Bain, G. M. Whitesides, *Langmuir* **1994**, 10, 1825.
- [35] S. C. Minne, G. Yaralioglu, S. R. Manalis, J. D. Adams, J. Zesch, A. Atalar, C. F. Quate, *Appl. Phys. Lett.* **1998**, 72, 2340.
- [36] P. Vettiger, G. Cross, M. Despont, U. Drechsler, U. Dürig, B. Gotsmann, W. Häberle, M. A. Lantz, H. E. Rothuizen, R. Stutz, G. K. Binnig, *IEEE Trans. Nanotechnol.* **2002**, 1, 39.
- [37] D. Bullen, S.-W. Chung, X. Wang, J. Zou, C. A. Mirkin, C. Liu, *Appl. Phys. Lett.* **2005**, 84, 789.
- [38] W. Cheng, E. Wang, *J. Phys. Chem. B* **2004**, 108, 24.